arXiv:1602.01425v1 [quant-ph] 3 Feb 2016

Geometric transformations of multidimensional color images based on NASS

Ping Fan[a,b], Ri-Gui Zhou[c,a,*], Naihuan Jing[b], Hai-Sheng Li[a]

[a] *School of Information Engineering, East China Jiaotong University, Nanchang, Jiangxi 330013, P.R. China*
[b] *Department of mathematics, North Carolina State University, Raleigh, NC 27695, USA*
[c] *College of Information Engineering, Shanghai Maritime University, Shanghai, 201306, P.R. China*

Abstract

We present quantum algorithms to realize geometric transformations (two-point swappings, symmetric flips, local flips, orthogonal rotations, and translations) based on an n-qubit normal arbitrary superposition state (NASS). These transformations are implemented using quantum circuits consisting of basic quantum gates, which are constructed with polynomial numbers of single-qubit and two-qubit gates. Complexity analysis shows that the global operators (symmetric flips, local flips, orthogonal rotations) can be implemented with $O(n)$ gates. The proposed geometric transformations are used to facilitate applications of quantum images with low complexity.

Keywords: geometric transformations, quantum image processing, quantum circuits, quantum computing

1. Introduction

Quantum computing is a combination of quantum mechanics and computer science. As a new computing paradigm, it offers one possible solution to the challenge posed by the failure of Moore's law [22]. Quantum computing [7] has several unique computational features such as quantum coherence, entanglement, and superposition of quantum states, which make quantum computing superior to its classical counterpart in information storage and parallel

*Corresponding author.
Email address: zrg@ecjtu.jx.cn (Ri-Gui Zhou)

computing [7]. Quantum algorithms such as the quantum Fourier transform [22, 24] are more efficient than their classical counterparts, as the quantum Fourier transform on 2^n elements can be performed with $O(n^2)$ gates, while the best classical analog, the Fast Fourier Transform(FFT), needs $O(n2^n)$ gates to implement [22]. Other famous quantum algorithms such as Shor's discrete logarithms and integer-factoring algorithms [24], Deutsch's parallel computing algorithm with quantum parallelism and coherence [4], and Grover's quadratic speed-up for an unordered database search algorithm [9, 32] have further shown the advantage of quantum computing over its classical counterpart. It has been an important problem to come up with quantum algorithms for known classical ones.

One reason that a quantum system is superior to a classical computer in information storage is due to the fact that the amplitude or phase of a quantum state can be used to store information [1]. In fact, if we consider a system of n qubits that stores 2^n complex numbers, for $n = 500$, 2^{500} is larger than the estimated number of atoms in the whole universe. Thus, trying to store all of these complex numbers would not be possible using any conceivable computer [22]. In a quantum system, if the frequency of the physical nature of a color represents its color instead of the RGB model or the HIS model [25, 26, 29], a color can be stored using only a 1-qubit quantum state [27] and an image may be stored as a quantum array [27, 28]. A flexible representation of quantum image (FRQI) state stores the colors and coordinates of a two-dimensional (2D) gray image with 2^n pixels using $(n + 1)$ qubits [15]. Maximally entangled qubits can be used to represent the vertices of polygons, so images can be reconstructed without using any additional information [28]. Information storage and retrieval were achieved based on the quantum amplitude in previous studies, but they can be also implemented based on the quantum phase [1].

Quantum computing is implemented via quantum gates. Universal quantum gates are expressed as combinations of single-qubit and two-qubit gates [22, 3], where two-qubit gates are universal in quantum computing [5]. In [21], an efficient scheme has been proposed for initializing a quantum register with an arbitrary superposed state and the application of the scheme to three specific cases was also discussed.

Many applications in both 2D and three-dimensional (3D) biomedical imaging require efficient techniques for geometric transformations of images [2, 6]. A polynomial interpolator structure is used for the high-quality geometric transformation of 2D and 3D images in a classical computer system [6].

In a quantum system, linear transformations [16, 11, 17], including two-point swappings, flips, orthogonal rotations, and restricted geometric transformations, are applied to 2D images based on their FRQI state. In addition, secure and efficient image processings for quantum computers have been described [12, 13], and these include quantum watermarking [11], quantum image encryption and decryption algorithms [10, 23, 30, 33].

An n-qubit normal arbitrary superposition state (NASS) can represent a k-dimensional color image (including pixels and colors) where n qubits encode the colors and coordinates of 2^n pixels (e.g., a five-dimensional color image of $1024 \times 1024 \times 1024 \times 1024 \times 1024$ using only 50 qubits) [19, 20]. Based on NASS and the color treatment strategy described in [18], we propose a new scheme to implement geometric transformations for multidimensional color images, including two-point swappings, symmetric flips, local flips, orthogonal rotations, and translations. The quantum circuit of a two-point swapping is designed using Gray codes. The quantum circuits of other geometric transformations are implemented in terms of two-point swapping circuits.

The remainder of this paper is organized as follows. Some basic quantum gate operations and a k-dimensional color image representation are described in Section 2. Geometric transformations for multidimensional color images are discussed in detail in Section 3. The simulated experiments are designed in Section 4. The conclusions are given in Section 5.

2. Basic quantum gates and representation of k-D color images

2.1. Quantum circuits

By the evolution postulate of quantum mechanics [22], the evolution of a closed quantum system is a reversible process. There are several well-known models of reversible quantum systems, and the notable ones are the quantum Turing machine [4], quantum circuit model [8], quantum cellular automation [14] and so on. These models are essentially equivalent [31], so we choose the easiest quantum circuit model to describe geometric transformations. A quantum circuit consists of a series of quantum gates to realize a specific function. Some quantum circuits are shown in Figure 1. These circuits are executed from left-to-right, and each line in the circuits represents a wire. Equivalently a quantum circuit is a realization of a unitary matrix.

2.2. Basic quantum gates

The state of a quantum system is described by a unit vector called *ket* in a Hilbert space. The left and right kets are denoted by $\langle\ |$ and $|\ \rangle$ respectively [22].

Let $|u\rangle$ and $|v\rangle$ be arbitrary two states given by

$$|u\rangle = \left[\begin{array}{ccc} u_0 & \cdots & u_{n-1} \end{array}\right]^T$$

and

$$|v\rangle = \left[\begin{array}{ccc} v_0 & \cdots & v_{n-1} \end{array}\right]^T$$

where $[\cdot]^T$ denotes the matrix transpose and $u_i, v_i \in \mathbb{C}$, the set of complex numbers.

The Hermitian conjugates of $|u\rangle$ and $|v\rangle$ are denoted by

$$\langle u| = |u\rangle^+ = \left[\begin{array}{ccc} u_0^+ & \cdots & u_{n-1}^+ \end{array}\right]$$

and

$$\langle v| = |v\rangle^+ = \left[\begin{array}{ccc} v_0^+ & \cdots & v_{n-1}^+ \end{array}\right]$$

where u_i^+ and v_i^+ are the complex conjugates.

The special states $|0\rangle$ and $|1\rangle$ are defined as

$$|0\rangle = \left[\begin{array}{c} 1 \\ 0 \end{array}\right],\ |1\rangle = \left[\begin{array}{c} 0 \\ 1 \end{array}\right].$$

The tensor product of column matrices is defined by

$$|u\rangle \otimes |v\rangle = \left[\begin{array}{ccccccc} u_0v_0 & \cdots & u_0v_{n-1} & \cdots & u_{n-1}v_0 & \cdots & u_{n-1}v_{n-1} \end{array}\right]^T$$

which is also written simply as $|u\rangle\,|v\rangle$ or $|uv\rangle$.

The n fold tensor product $U \otimes U \otimes \cdots \otimes U$ of the operator U is abbreviated as $U^{\otimes n}$. Similarly $|u\rangle \otimes |u\rangle \cdots \otimes |u\rangle$ is expressed as $|u\rangle^{\otimes n}$.

A linear operator A is unitary if $AA^+ = A^+A = I$, where A^+ is the conjugate transpose of A and I is the identity operator shown in Figure 1.

Some of the basic gates and their corresponding matrices are shown in Figure 1. The identity (I), Hadamard (H), and Pauli-X (X) gates are well-known and can be found in the basic reference [22]. The gates U, U_{C1}, U_{C0}, and $C^n(U)$ are the fourth, fifth, sixth, and seventh gates in Figure 1. They are defined as follows.

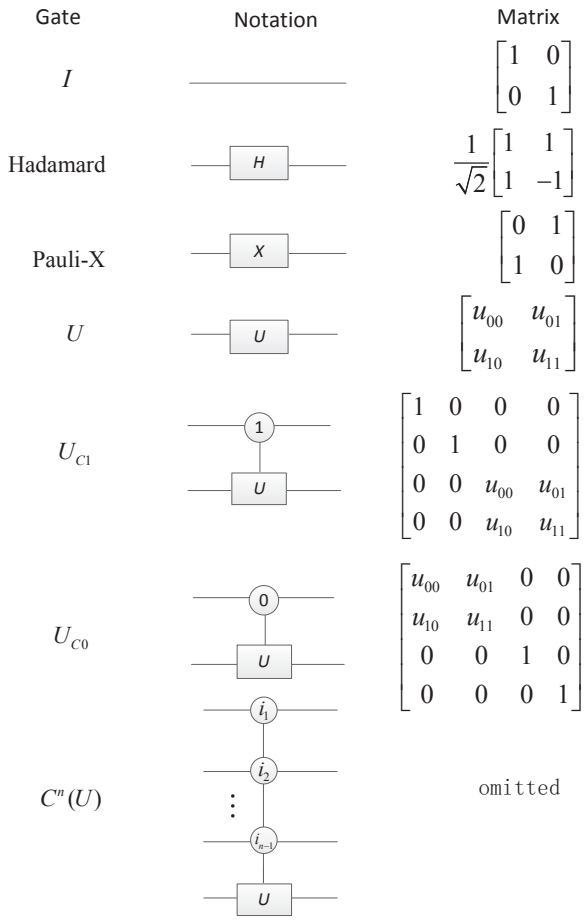
Gate
Notation
Matrix
I
$\begin{bmatrix} 1 & 0 \\ 0 & 1 \end{bmatrix}$
Hadamard
H
$\frac{1}{\sqrt{2}}\begin{bmatrix} 1 & 1 \\ 1 & -1 \end{bmatrix}$
Pauli-X
X
$\begin{bmatrix} 0 & 1 \\ 1 & 0 \end{bmatrix}$
U
U
$\begin{bmatrix} u_{00} & u_{01} \\ u_{10} & u_{11} \end{bmatrix}$
U_{C1}
1
U
$\begin{bmatrix} 1 & 0 & 0 & 0 \\ 0 & 1 & 0 & 0 \\ 0 & 0 & u_{00} & u_{01} \\ 0 & 0 & u_{10} & u_{11} \end{bmatrix}$
U_{C0}
0
U
$\begin{bmatrix} u_{00} & u_{01} & 0 & 0 \\ u_{10} & u_{11} & 0 & 0 \\ 0 & 0 & 1 & 0 \\ 0 & 0 & 0 & 1 \end{bmatrix}$
$C^n(U)$
i_1
i_2
i_{n-1}
U
omitted

Figure 1: Notations for some basic gates with their corresponding matrices. The operator U is unitary and the gate $C^n(U)$ is associated with $i_1, i_2, \ldots, i_{n-1} \in \{0, 1\}$.

Let $|\psi\rangle$ and $|\xi\rangle$ be two arbitrary states

$$\begin{cases} |\psi\rangle = \alpha\,|0\rangle + \beta\,|1\rangle \\ |\xi\rangle = c\,|0\rangle + d\,|1\rangle \end{cases}, \qquad \alpha, \beta, c, d \in \mathbb{C} \tag{1}$$

Then the action of U is given by

$$U\,|\psi\rangle = (\alpha u_{00} + \beta u_{01})\,|0\rangle + (\alpha u_{10} + \beta u_{11})\,|1\rangle \tag{2}$$

When U is the Pauli-X gate, Eq. (2) becomes

$$X\,|\psi\rangle = X(\alpha\,|0\rangle + \beta\,|1\rangle) = \beta\,|0\rangle + \alpha\,|1\rangle \tag{3}$$

Apply the U_{C1} and U_{C0} gates to the states $|\psi\rangle$ and $|\xi\rangle$ in Eq. (1), respectively:

$$U_{C1}(\,|\xi\rangle\,|\psi\rangle) = c\,|0\rangle\,|\psi\rangle + d\,|1\rangle\,(U\,|\psi\rangle) \tag{4}$$

and

$$U_{C0}(\,|\xi\rangle\,|\psi\rangle) = c\,|0\rangle\,(U\,|\psi\rangle) + d\,|1\rangle\,|\psi\rangle \tag{5}$$

where $U\,|\psi\rangle$ is shown in Eq. (2).

When U is the Pauli-X gate, then U_{C1} and U_{C0} are designated as N_{C1} and N_{C0}, respectively, which are also called the controlled-NOT, as shown in Figure 2. Therefore,

$$N_{C1}(\,|\phi\rangle\,|\psi\rangle) = c\,|0\rangle\,|\psi\rangle + d\,|1\rangle\,(X\,|\psi\rangle) \tag{6}$$

and

$$N_{C0}(\,|\phi\rangle\,|\psi\rangle) = c\,|0\rangle\,(X\,|\psi\rangle) + d\,|1\rangle\,|\psi\rangle \tag{7}$$

The $C^n(U)$ $(n \geq 3)$ gate associated with $i_1, \cdots, i_{n-1} \in \{0, 1\}$ acts on the n-fold tensor product of the Hilbert space. Its action on the tensor product of n one-qubit states $|x_1 x_2 \cdots x_{n-1}\rangle\,|\psi\rangle$ is given by

$$\begin{array}{l} C^n(U)(|x_1 x_2 \cdots x_{n-1}\rangle\,|\psi\rangle) \\ = |x_1 \cdots x_{n-1}\rangle\,U^{f(x_1 \cdots x_{n-1}, i_1 \cdots i_{n-1})}\,|\psi\rangle \end{array} \tag{8}$$

where the function $f = f(x_1 \cdots x_{n-1}, i_1 \cdots i_{n-1})$ is defined by

$$\left\{ \begin{array}{ll} f(x_1 \cdots x_{n-1}, i_1 \cdots i_{n-1}) = 0, & x_1 \cdots x_{n-1} = i_1 \cdots i_{n-1} \\ f(x_1 \cdots x_{n-1}, i_1 \cdots i_{n-1}) = 1, & x_1 \cdots x_{n-1} \neq i_1 \cdots i_{n-1} \end{array} \right. \tag{9}$$

For $k = 1, \cdots, n$, one also defines the gate $C^n(U_k)$ as the composition of $C^n(U)$ and the permutation operator $P_{k,n}$, which switches the kth and nth factors of arbitrary tensor product of n one-qubits:

$$P_{k,n}|j_1 \cdots j_k \cdots j_n\rangle = |j_1 \cdots j_n \cdots j_k\rangle.$$

In particular, for the Pauli X-gate, the gate $C^n(X_k)$ $(k = 1, 2, \cdots, n)$ associated with $i_1, \cdots, i_{n-1} \in \{0, 1\}$ is shown in Figure 3. Its exact action on the tensor product $|j_1 \cdots j_{k-1} j_k j_{k+1} \cdots j_n\rangle$ is given by

$$\begin{array}{l} C^n(X_k)\,|j_1 \cdots j_{k-1} j_k j_{k+1} \cdots j_n\rangle \\ = |j_1 \cdots j_{k-1}\rangle\,(X^f\,|j_k\rangle)\,|j_{k+1} \cdots j_n\rangle \end{array} \tag{10}$$

where $f = f(j_1 \cdots j_{k-1} j_{k+1} \cdots j_n, i_1 \cdots i_{n-1})$ is defined in Eq. (9). For example, when $n = 3$ and $i_1 = i_3 = 1$, we have $C^3(X_2)\,|111\rangle = |101\rangle$.

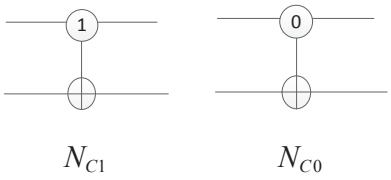

Figure 2: Two controlled-NOT gates.

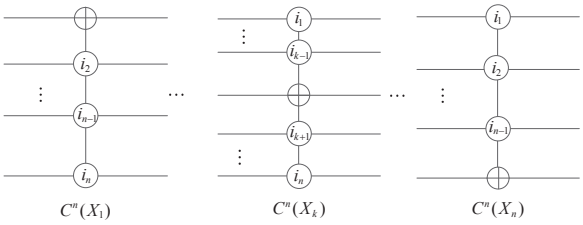

Figure 3: Set of n_k-qubit controlled-NOT gates ($k = 1, 2, \cdots, n$).

2.3. Representation of a quantum image

We recall how NASS represents a multidimensional color image [20].

Suppose there are M colors and $Color = \{color_1, color_2, \cdots, color_M\}$ is a sorted set of the colors. We convert the ith color to an angle value by

$$\phi_i = \frac{\pi(i-1)}{2(M-1)} \tag{11}$$

where $1 \leqslant i \leqslant M$. This establishes a one-to-one correspondence F_1 between the sorted color set and a sorted angle set $\phi = \{\phi_1, \phi_2, \cdots, \phi_M\}$. For RGB color images, $M = 2^{24}$, let x, y, z be the values of R, G, B in 24-bit RGB True Color, and let $i = x \times 256 \times 256 + y \times 256 + z + 1$. Thus, $color_i$ corresponds to the value (x, y, z) of RGB. For instance, $color_1$ and $color_{16777216}$ correspond to the RGB values (0,0,0) and (255,255,255) respectively.

By a k-dimensional color image, we mean a k-dimenisional lattice of size $2^{m_1} \times 2^{m_2} \times \cdots \times 2^{m_k}$, where each lattice point is painted with a color. For simplicity we often assume that the image has spread out the full range of $0, 1, \cdots, 2^{m_i} - 1$ in the ith axis, and if the actual size is less, we can take the color to be empty in the remaining spots, and then we enlarge the color set by the empty color. We only consider the n-dimensional skeleton situated in the positive direction of each axis. Let $n = m_1 + m_2 + \ldots + m_k$, then we assign the image a quantum superposition state in the 2^n-dimensional

Hilbert space:

$$|\psi_\phi\rangle_k = \sum_{i=0}^{2^n-1} a_i |i\rangle = \sum_{i=0}^{2^n-1} a_i |v_1\rangle |v_2\rangle \cdots |v_k\rangle \tag{12}$$

where $|v_1\rangle, |v_2\rangle, \ldots, |v_k\rangle$ correspond to the k axes of the image respectively and a_i is the angle value at the site i. The running index i goes through all lattice points of the image, and $i = i_1 i_2 \cdots i_n$ is its binary expansion obtained by taking the superposition of $v_1, v_2, \cdots, v_k$, where $v_1 = i_1 \cdots i_{m_1}$, $v_2 = i_{m_1+1} \cdots i_{m_1+m_2}$ and $v_k = i_{n-m_k+1} \cdots i_n$ are in their binary expansions. Thus $|i\rangle = |v_1\rangle |v_2\rangle \cdots |v_k\rangle$ is the coordinate $(v_1, v_2, \cdots, v_k)$ of i in the k-dimensional space and $a_i \in \phi$ is the value of the color at site i.

We define the NASS state of the image to be the normalized state

$$|\psi\rangle_k = \sum_{i=0}^{2^n-1} \theta_i |v_1\rangle |v_2\rangle \cdots |v_k\rangle \tag{13}$$

where $\theta_i = a_i / \sqrt{\sum_{y=0}^{2^n-1} a_y^2}$. Note that the magnitude square $\sum_{y=0}^{2^n-1} a_y^2$ is a constant for the image, so θ_i can replace a_i to represent the color at the site i. In this way the NASS state $|\psi\rangle_k$ in Eq. (13) represents a k-dimensional color image.

Each axis $|v_i\rangle$ spans a Hilbert space of dimension 2^{m_i}. In view of its role in the image, we abuse the notation to denote $\dim(|v_i\rangle) = m_i$ and also call it the size of the state $|v_i\rangle$. e.g., $\dim(|000\rangle) = 3$, and we have

$$\dim(|\psi\rangle_k) = \sum_{i=1}^{k} \dim(|v_i\rangle) = n \tag{14}$$

where $|\psi\rangle_k$ is the NASS state shown in Eq. (13).

To make Eq. (13) clearer, let us consider $\dim(|v_i\rangle) = m_i$, $i = 1, 2, \ldots, k$ as an example. The NASS state representing a multidimensional color image with 2^n pixels is written explicitly as follows.

$$\begin{aligned} |\psi\rangle_k = \sum_{i=0}^{2^n-1} \theta_i |i_1 \cdots i_{m_1}\rangle \cdots \Big| i_{(\sum_{h=1}^{j-1} m_h)+1} \cdots i_{(\sum_{h=1}^{j-1} m_h)+m_j} \Big\rangle \\ \cdots \Big| i_{(\sum_{h=1}^{k-1} m_h)+1} \cdots i_{(\sum_{h=1}^{k} m_h)} \Big\rangle \end{aligned} \tag{15}$$

where $1 \leq j \leq k$ and the binary expansion of the integer i is

$$\begin{aligned} i = i_1 \cdots i_{m_1} \cdots i_{\substack{j-1 \\ (\sum_{h=1} m_h)+1}} \cdots i_{\substack{j-1 \\ (\sum_{h=1} m_h)+m_j}} \\ \cdots i_{\substack{k-1 \\ (\sum_{h=1} m_h)+1}} \cdots i_{\substack{k-1 \\ (\sum_{h=1} m_h)+m_k}} \end{aligned} \tag{16}$$

Substituting $n = 5$, $k = 2$, $m_1 = 2$ and $m_2 = 3$ into Eq. (15), we obtain

$$\begin{aligned} |\psi\rangle_2 = \sum_{i=0}^{2^5-1} \theta_i |i_1 i_2\rangle |i_3 i_4 i_5\rangle = \theta_0 |00\rangle |000\rangle \\ + \theta_1 |00\rangle |001\rangle + \cdots + \theta_{30} |11\rangle |110\rangle + \theta_{31} |11\rangle |111\rangle \end{aligned} \tag{17}$$

which represents the 2D color image shown in Figure 4.

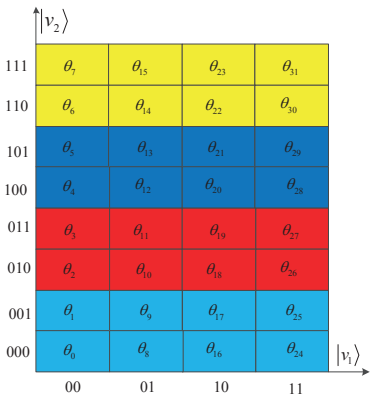

Figure 4: Two-dimensional color image of 4×8.

Substituting $n = 5$, $k = 3$, $m_1 = 2$, $m_2 = 2$ and $m_3 = 1$ into Eq. (15), we obtain

$$\begin{aligned} |\psi\rangle_3 = \sum_{i=0}^{2^5-1} \theta_i |i_1 i_2\rangle |i_3 i_4\rangle |i_5\rangle = \theta_0 |00\rangle |00\rangle |0\rangle \\ + \theta_1 |00\rangle |00\rangle |1\rangle + \cdots + \theta_{30} |11\rangle |11\rangle |0\rangle + \theta_{31} |11\rangle |11\rangle |1\rangle \end{aligned} \tag{18}$$

which represents the 3D color image shown in Figure 5.

Substituting $n = 5$, $k = 5$, and $m_1 = m_2 = m_3 = m_4 = m_5 = 1$ into Eq. (15), we obtain

$$\begin{aligned} |\psi_5\rangle = \sum_{i=0}^{2^5-1} \theta_i |i_1\rangle |i_2\rangle |i_3\rangle |i_4\rangle |i_5\rangle \\ = \theta_0 |0\rangle |0\rangle |0\rangle |0\rangle |0\rangle + \theta_1 |0\rangle |0\rangle |0\rangle |0\rangle |1\rangle \\ + \cdots + \theta_{30} |1\rangle |1\rangle |1\rangle |1\rangle |0\rangle + \theta_{31} |1\rangle |1\rangle |1\rangle |1\rangle |1\rangle \end{aligned} \tag{19}$$

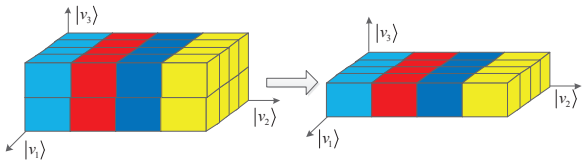

Figure 5: 3D color image of $4 \times 4 \times 2$. In the lower sub-image on the right-hand side, $|i_5\rangle = |0\rangle$.

which represents the five-dimensional (5D) color image shown in Figure 6.

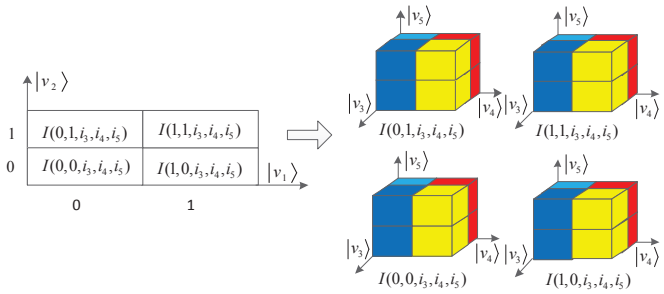

Figure 6: 5D color image of $2 \times 2 \times 2 \times 2 \times 2$. The image is divided into four sub-images, i.e., $I(0,0,i_3,i_4,i_5)$, $I(0,1,i_3,i_4,i_5)$, $I(1,0,i_3,i_4,i_5)$, and $I(1,1,i_3,i_4,i_5)$. The projections of the four sub-images into the 3D space spanned by $|v_3\rangle \times |v_4\rangle \times |v_5\rangle$ are shown on the right.

3. Geometric transformations for multidimensional color images

Geometric transformations on quantum images [16], such as two-point swappings, flips, and orthogonal rotations, can be applied to 2D images based on the FRQI state. Using [16, 17], we discuss geometric transformations for multidimensional color images based on the NASS state.

3.1. Two-point swappings

Definition 1. *A two-point swapping G_T for a k-dimensional image is the linear operator defined by*

$$G_T = |s\rangle\langle t| + |t\rangle\langle s| + \sum_{i=0, i\neq s,t}^{2^n-1} |i\rangle\langle i| \tag{20}$$

where $|\mathrm{s}\rangle = |v_1^s\rangle\,|v_2^s\rangle\cdots|v_k^s\rangle$ *and* $|t\rangle = |v_1^t\rangle\,|v_2^t\rangle\cdots|v_k^t\rangle$ *are the coordinates of the two swapped pixels, and* $|i\rangle = |v_1\rangle\,|v_2\rangle\cdots|v_k\rangle$ *run through the coordinates of the other pixels.*

Since $G_T.G_T^+ = I^{\otimes n}$, G_T is a unitary operator. Applying G_T to the NASS state $|\psi\rangle_k$ in Eq. (13), we get

$$\begin{aligned} G_T(|\psi\rangle_k) &= \sum_{i=0}^{2^n-1} \theta_i G_T(|i\rangle) \\ &= \theta_s\,|t\rangle + \theta_t\,|s\rangle + \sum_{i=0, i\neq s,t}^{2^n-1} \theta_i\,|i\rangle \end{aligned} \tag{21}$$

That is, G_T swaps two colors of a k-dimensional color image. We can use Gray codes [22] to design a quantum circuit for the operator G_T of two-point swapping. Suppose that s and t are two distinct binary numbers, then a Gray code connecting s and t is a sequence of binary numbers that starts with s and ends with t such that adjacent binary numbers in the list differ by exactly one bit. For example, a Gray code connecting $s = 0\cdots0\cdots0$ and $t = 1\cdots1\cdots1$ is

$$\begin{array}{ccccc} 0 & \cdots & 0 & \cdots & 0 \\ 0 & \cdots & 0 & \cdots & 1 \\ \vdots & & \vdots & & \vdots \\ 0 & \cdots & 1 & \cdots & 1 \\ \vdots & & \vdots & & \vdots \\ 1 & \cdots & 1 & \cdots & 1 \end{array} \tag{22}$$

Suppose s and t are two binary numbers with at most n digits different. Then we can find a Gray code $g_1, g_2, \ldots, g_m$ to connect s and t with $m(\leq n+1)$ elements, where $g_1 = s$ and $g_m = t$. Since the elements g_i and g_{i+1} $(1 \leq i \leq m-1)$ differ at only one location, we can implement the transformation $|g_i\rangle \rightarrow |g_{i+1}\rangle$ by the $C^n(X_k)$ gate shown in Figure 3. For example, when $|g_2\rangle = |0\cdots01\rangle$ and $|g_3\rangle = |0\cdots11\rangle$, where $|g_2\rangle$ and $|g_3\rangle$ are two elements of the Gray code in Eq. (22), the $C^n(X_{n-1})$ gate in Figure 3 sends $|g_2\rangle$ to $|g_3\rangle$.

To understand implementation of the quantum circuits for two-point swapping more clearly, let us consider a k-dimensional color image with 2^n pixels as an example. Suppose that the NASS state $|\psi\rangle_k$ in Eq. (15) represents the image. In addition, assume that $|s\rangle = |0\rangle$ and $|t\rangle = |2^n-1\rangle$ are the coordinates of the two swapped pixels. The Gray code that connects

s and t is shown in Eq. (22), where $g_1, g_2, \ldots g_{n+1}$ are the elements of the Gray code, $|g_1\rangle = |s\rangle = |0\rangle$, and $|g_{n+1}\rangle = |t\rangle = |2^n - 1\rangle$. We can achieve the two-point swapping of the k-dimensional color image by implementing the transformations as follows (a proof is given in Appendix A).

$$\begin{cases} |g_1\rangle \rightarrow |g_2\rangle \rightarrow \cdots \rightarrow |g_{n+1}\rangle \\ |g_n\rangle \rightarrow |g_{n-1}\rangle \rightarrow \cdots \rightarrow |g_1\rangle \end{cases} \tag{23}$$

The quantum circuit for the transformations in Eq. (23) is shown in Figure 7.

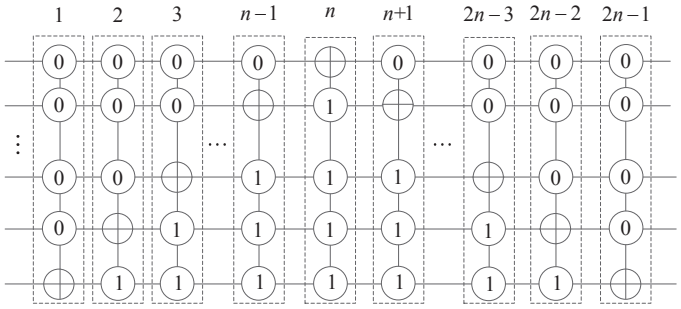

Figure 7: The implementation of a two-point swapping of a k-dimensional color image, where the coordinates of two points are $|0\rangle$ and $|2^n - 1\rangle$. The dashed box i ($1 \leq i \leq n$) and $n + j$ ($1 \leq j \leq n - 1$) implement the transformations $|g_i\rangle \rightarrow |g_{i+1}\rangle$ and $|g_{n+1-j}\rangle \rightarrow |g_{n-j}\rangle$, respectively.

Since there are more than one Gray codes connecting s and t, the implementation of the two-point swapping of s and t can be done by more than one quantum circuits. For example, if $s = 00101$ and $t = 11110$, two Gray codes are as follows.

$$\begin{array}{ccccc} 0 & 0 & 1 & 0 & 1 \\ 1 & 0 & 1 & 0 & 1 \\ 1 & 1 & 1 & 0 & 1 \\ 1 & 1 & 1 & 1 & 1 \\ 1 & 1 & 1 & 1 & 0 \end{array} \tag{24}$$

and

$$\begin{array}{ccccc} 0 & 0 & 1 & 0 & 1 \\ 0 & 0 & 1 & 0 & 0 \\ 0 & 0 & 1 & 1 & 0 \\ 0 & 1 & 1 & 1 & 0 \\ 1 & 1 & 1 & 1 & 0 \end{array} \tag{25}$$

Using the Gray code in Eq. (24), we can implement the two-point swapping of the 3D color image in Figure 5, where the coordinates of the two pixels are $|s\rangle = |00\rangle\,|10\rangle\,|1\rangle$ and $|t\rangle = |11\rangle\,|11\rangle\,|0\rangle$, i.e., $(0, 2, 1)$ and $(3, 3, 0)$. The quantum circuit and the result of the two-point swapping are shown in Figure 8.

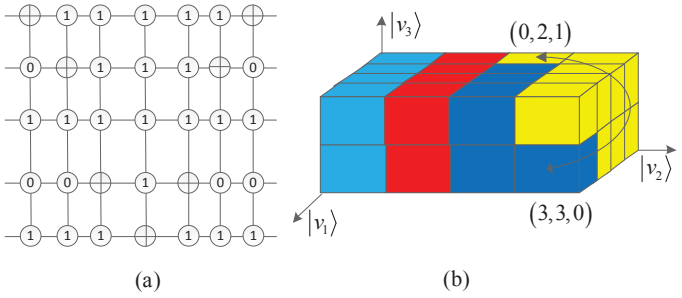

Figure 8: Implementation of the two-point swapping of a 3D color image. (a) The quantum circuit for two-point swapping. (b) The swapped image.

Similarly, we employ the Gray code in Eq. (25) to achieve the swapping of $|00101\rangle$ (i.e., (0,0,1,0,1)) and $|11110\rangle$ (i.e., (1,1,1,1,0)) in the 5D color image in Figure 6. The quantum circuit and the result of the two-point swapping are shown in Figure 9.

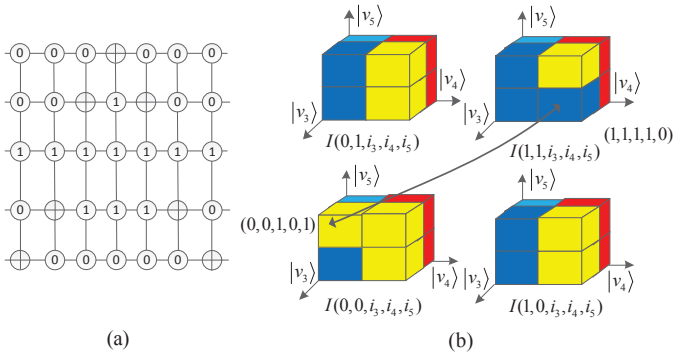

Figure 9: Implementation of the two-point swapping of a 5D color image. (a) The quantum circuit for two-point swapping. (b) The swapped image.

As any quantum circuit can be built using single-qubit and controlled-NOT gates [22], we introduce the following notion.

Definition 2. *The complexity of a quantum circuit is the total number of single-qubit and controlled-NOT gates (i.e., N_{C1} in Figure 2)) in the quantum circuit.*

Theorem 1. *Let $s = g_1, g_2, \cdots, g_m = t$ be the n-bit elements of a Gray code connecting s and t, where $|s\rangle$ and $|t\rangle$ are the coordinates of the two swapped pixels in G_T. The transformations $|g_1\rangle \to |g_2\rangle \to \cdots \to |g_m\rangle$ and $|g_{m-1}\rangle \to |g_{m-2}\rangle \to \cdots \to |g_1\rangle$ can be achieved by a sequence of $C^n(X_k)$ gates as shown in Figure 3. The final result is an implementation of two-point swapping operators G_T with complexity $O(n^2)$.*

Proof. See Appendix A. □

3.2. Flip transformations

For any vector $|v\rangle = |j_1 j_2 \cdots j_m\rangle$, we define $|\overline{v}\rangle = |\bar{j}_1 \bar{j}_2 \cdots \bar{j}_m\rangle$, where $\bar{j}_h = 1 - j_h$, $h = 1, 2, \cdots m$.

Definition 3. *A symmetric flip $G_F^{|v_j\rangle}$ for the NASS state $|\psi\rangle_k$ along the $|v_j\rangle$ axis is the linear operator*

$$G_F^{|v_j\rangle}(|\psi\rangle_k) = \sum_{i=0}^{2^n-1} \theta_i \left|\overline{v_1}\right\rangle \cdots \left|\overline{v_{j-1}}\right\rangle |v_j\rangle \left|\overline{v_{j+1}}\right\rangle \cdots \left|\overline{v_k}\right\rangle \tag{26}$$

where $|\psi\rangle_k$ is a k-dimensional color image (see Eq. (13)), $|v_1\rangle, \ldots, |v_k\rangle$ are the k axes in a k-dimensional space.

For example, by applying $G_F^{|v_j\rangle}$ to the NASS state $|\psi\rangle_k$ in Eq. (15), the result is

$$\begin{aligned} & G_F^{|v_j\rangle}(|\psi\rangle_k) \\ & = \sum_{i=0}^{2^n-1} \theta_i \left|\bar{i}_1 \cdots \bar{i}_{m_1}\right\rangle \cdots \left| i_{(\sum_{h=1}^{j-1} m_h)+1} \cdots i_{(\sum_{h=1}^{j-1} m_h)+m_j} \right\rangle \\ & \cdots \left| \bar{i}_{(\sum_{h=1}^{k-1} m_h)+1} \cdots \bar{i}_{(\sum_{h=1}^{k-1} m_h)+m_k} \right\rangle \end{aligned} \tag{27}$$

where $\dim(|v_l\rangle) = m_l$, $l = 1, 2, \ldots, k$.

The symmetric flip $G_F^{|v_j\rangle}$ in Eq. (27) is also expressed as

$$G_F^{|v_j\rangle} = X^{\otimes m_1} \otimes \cdots X^{\otimes m_{j-1}} \otimes I^{\otimes m_j} \otimes X^{\otimes m_{j+1}} \cdots \otimes X^{\otimes m_k} \tag{28}$$

where X is the Pauli spin operator (see Figure 1). The implementation of the operator $G_F^{|v_j\rangle}$ in Eq. (28) is shown in Figure 10. Suppose that $n-\dim(|v_j\rangle) = m$, we know that the implementation of the operator $G_F^{|v_j\rangle}$ requires m Pauli-X gates, where $m < n$, i.e., the complexity of the operator $G_F^{|v_j\rangle}$ is $O(n)$.

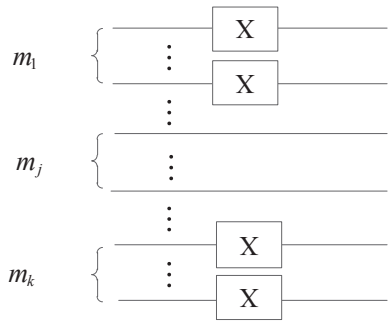

Figure 10: Implementation of the operator $G_F^{|v_j\rangle}$.

Substituting $n = 5$, $k = 5$, $j = 1$, and $m_1 = m_2{=}m_3{=}m_4{=}m_5{=}\ 1$ into Eq. (27), we obtain

$$\begin{aligned} G_F^{|v_1\rangle}(|\psi\rangle_k) &= \sum_{i=0}^{2^n-1} \theta_i \,|i_1\rangle\,|\bar{i}_2\rangle\,|\bar{i}_3\rangle\,|\bar{i}_4\rangle\,|\bar{i}_5\rangle \\ &= \theta_0\,|0\rangle\,|1\rangle\,|1\rangle\,|1\rangle\,|1\rangle + \theta_1\,|0\rangle\,|1\rangle\,|1\rangle\,|1\rangle\,|0\rangle \\ &+ \cdots + \theta_{31}\,|1\rangle\,|0\rangle\,|0\rangle\,|0\rangle\,|0\rangle \end{aligned} \tag{29}$$

which implements a symmetric flip of a 5D color image. This is shown in part (a) of Figure 11.

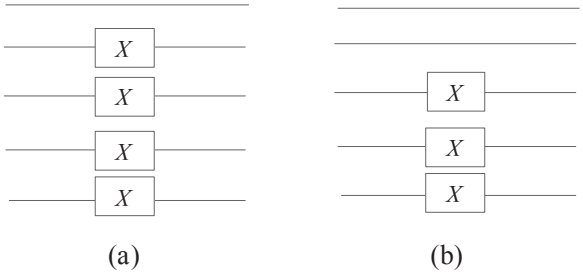

Figure 11: Implementation of the operator $G_F^{|v_1\rangle}$. (a) $G_F^{|v_1\rangle}$ is in Eq. (29). (b) $G_F^{|v_1\rangle}$ is in Eq. (30).

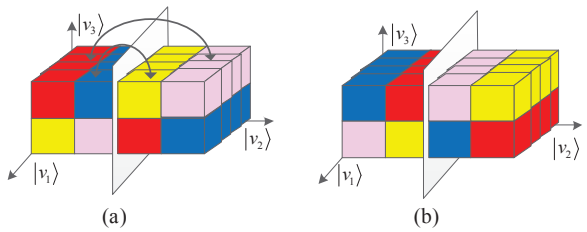

Figure 12: Symmetry flip of a 3D color image along the $|v_1\rangle$ axis. (a) The original image. (b) The transformed image.

Substituting $n = 5$, $k = 3$, $j = 1$, $m_1 = 2$, $m_2 = 2$, and $m_3 = 1$ into Eq. (27), we obtain

$$\begin{aligned} &G_F^{|v_1\rangle}(|\psi\rangle_3) = \sum_{i=0}^{2^n-1} \theta_i \left|i_1 i_2\right\rangle \left|\bar{i}_3 \bar{i}_4\right\rangle \left|\bar{i}_5\right\rangle \\ &= \theta_0 \left|00\right\rangle \left|11\right\rangle \left|1\right\rangle + \theta_1 \left|00\right\rangle \left|11\right\rangle \left|0\right\rangle + \cdots + \theta_{31} \left|11\right\rangle \left|00\right\rangle \left|0\right\rangle \end{aligned} \tag{30}$$

which realizes a symmetric flip of a 3D color image and is shown in part (b) of Figure 11. Application of the quantum circuit to the image in Figure 5 is shown in Figure 12.

Theorem 2. *The operator $G_F^{|v_j\rangle}$ can be implemented by 2^{n-1} two-point swappings in Eq. (20). The quantum circuit is reduced to the one shown in Figure 10, and the complexity of the symmetric flip is $O(n)$.*

Proof. See Appendix B. □

Definition 4. *A local flip $G_{LF}^{|v_x\rangle v(j,h,m)}$ for the NASS state $|\psi\rangle_k$ along the $|v_x\rangle$ axis is defined as the operator*

$$\begin{aligned} &G_{LF}^{|v_x\rangle v(j,h,m)}(|\psi\rangle_k) = \sum_{i=0, j_h \neq m}^{2^n-1} \theta_i \left|v_1\right\rangle \cdots \left|v_k\right\rangle \\ &+ \sum_{i=0, j_h = m}^{2^n-1} (\theta_i \left|\overline{v_1}\right\rangle \cdots \left|\overline{v_{j-1}}\right\rangle \left|\bar{j}_1 \cdots \bar{j}_{h-1} j_h \bar{j}_{h+1} \cdots \bar{j}_{m_j}\right\rangle \\ &\left|\overline{v_{j+1}}\right\rangle \cdots \left|\overline{v_{x-1}}\right\rangle \left|v_x\right\rangle \left|\overline{v_{x+1}}\right\rangle \cdots \left|\overline{v_k}\right\rangle) \end{aligned} \tag{31}$$

where $|\psi\rangle_k$ represents a k-dimensional color image (see Eq. (13)), and $|v_1\rangle, \ldots, |v_k\rangle$ are the k axes.

Here $v(j,h,m)$ means that for the axis $|v_j\rangle = \left|j_1 \cdots j_h \cdots j_{m_j}\right\rangle$, when $j_h \neq m$, the corresponding pixels are not transformed. When $j_h = m$, the

corresponding pixels are flipped. Suppose that $|v_l\rangle = |j_1 j_2 \cdots j_{m_l}\rangle$, then $|\overline{v_l}\rangle = |\bar{j}_1 \bar{j}_2 \cdots \bar{j}_{m_l}\rangle$, $\bar{j}_h = 1 - j_h$, $h = 1, 2, \cdots m_l$.

For example, application of $G_{LF}^{|v_x\rangle v(j,h,m)}$ to the NASS state $|\psi\rangle_k$ in Eq. (15) is

$$\begin{aligned} & G_{LF}^{|v_x\rangle v(j,h,m)}(|\psi\rangle_k) \\ &= \sum_{i=0, j_h \neq m}^{2^n-1} \theta_i \, |i_1 \cdots i_{m_1}\rangle \cdots |i_{l_k+1} \cdots i_{l_k+m_k}\rangle \\ &+ \sum_{i=0, j_h = m}^{2^n-1} \theta_i \, |\bar{i}_1 \cdots \bar{i}_{m_1}\rangle \cdots \left|\bar{j}_1 \cdots \bar{j}_{h-1} j_h \bar{j}_{h+1} \cdots \bar{j}_{m_j}\right\rangle \\ &\cdots |i_{l_x+1} \cdots i_{l_x+m_x}\rangle \cdots |\bar{i}_{l_k+1} \cdots \bar{i}_{l_k+m_k}\rangle \end{aligned} \tag{32}$$

where $m_y = \dim(|v_y\rangle)$, $y = 1, 2, \ldots, k$, $l_l = m_1 + m_2 + \cdots + m_{l-1}$, $l = 2, \ldots, k$.

The implementation of $G_{LF}^{|v_x\rangle v(j,h,m)}$ is shown in Figure 13. From Figure 13, we know that $G_{LF}^{|v_x\rangle v(j,h,m)}$ is implemented by $n - 1 - \dim(|v_x\rangle)$ N_{C1} or the N_{C0} gates in Figure 2, i.e., the complexity of the operator $G_{LF}^{|v_x\rangle v(j,h,m)}$ is $O(n)$.

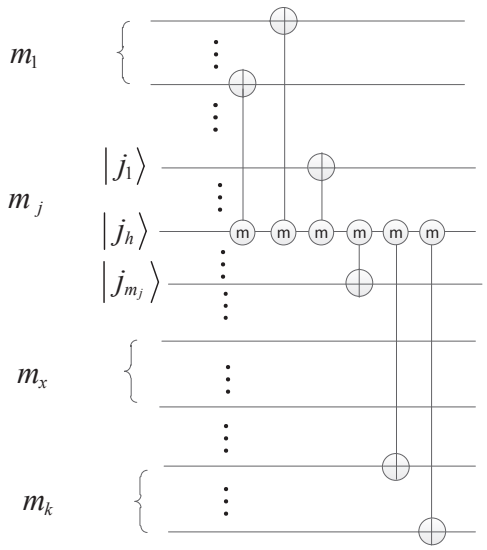

Figure 13: Implementation of the operator $G_{LF}^{|v_x\rangle v(j,h,m)}$ where $m = 0$ or $m = 1$.

Substituting $n = 5$, $k = 5$, $x = 1$, $v(j,h,m) = v(2,1,1)$ and $m_1 =$

m_2=m_3=m_4=m_5= 1 into Eq. (32), we obtain

$$\begin{aligned} &G_{LF}^{|v_1\rangle v(2,1,1)}(|\psi\rangle_5) \\ &= \sum_{i=0}^{31} \theta_i \left|i_1\right\rangle \left|0\right\rangle \left|i_3\right\rangle \left|i_4\right\rangle \left|i_5\right\rangle + \sum_{i=0}^{31} \theta_i \left|i_1\right\rangle \left|1\right\rangle \left|\bar{i}_3\right\rangle \left|\bar{i}_4\right\rangle \left|\bar{i}_5\right\rangle \end{aligned} \tag{33}$$

Thus, we have implemented a local flip of a 5D color image. The implementation of the operator $G_{LF}^{|v_1\rangle v(2,1,1)}$ in Eq. (33) is shown in part (a) of Figure 14.

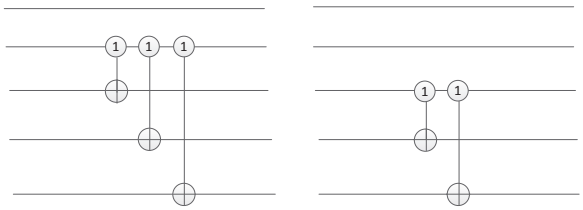

Figure 14: Two implementation circuits for a local flip. (a) The implementation circuit for $G_{LF}^{|v_1\rangle v(2,1,1)}$ in Eq. (33). (b) The implementation circuit for $G_{LF}^{|v_1\rangle v(2,1,1)}$ in Eq. (34).

Substituting $n = 5$, $k = 3$, $x = 1$, $m_1 = 2$, $m_2 = 2$, $m_3 = 1$, and $v(j, h, m) = v(2, 1, 1)$ into Eq. (32), we obtain

$$\begin{aligned} &G_{LF}^{|v_1\rangle v(2,1,1)}(|\psi\rangle_3) \\ &= \sum_{i=0}^{31} \theta_i \left|i_1 i_2\right\rangle \left|0 i_4\right\rangle \left|i_5\right\rangle + \sum_{i=0}^{31} \theta_i \left|i_1 i_2\right\rangle \left|1 \bar{i}_4\right\rangle \left|\bar{i}_5\right\rangle \end{aligned} \tag{34}$$

which implements a symmetric flip of a 3D color image. See part (b) of Figure 14 for the diagram. The application of the local flip to the image in Figure 5 is shown in Figure 15.

3.3. Orthogonal rotations

Definition 5. *An orthogonal rotation $R_{|v_x\rangle\otimes|v_y\rangle}^{\alpha}$ for the NASS state $|\psi\rangle_k$ along the plane spanned by $|v_x\rangle \otimes |v_y\rangle$ is defined as*

$$R_{|v_x\rangle\otimes|v_y\rangle}^{\alpha}(|\psi\rangle_k) = \sum_{i=0}^{2^n-1} \theta_i \left|v_1\right\rangle \cdots \left|v_x{}'\right\rangle \cdots \left|v_y{}'\right\rangle \cdots \left|v_k\right\rangle \tag{35}$$

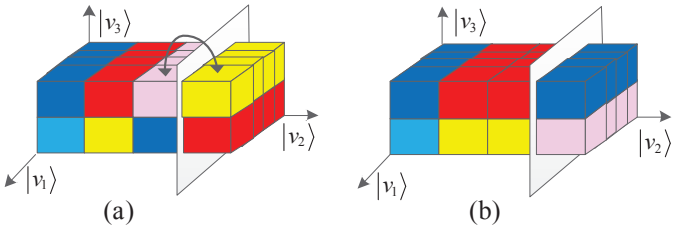

Figure 15: Local flip of a 3D color image. (a) The original image. (b) The transformed image.

where $|\psi\rangle_k$ *is a k-dimensional color image (see Eq. (13)),* $\alpha \in \left\{\frac{\pi}{2}, \pi, \frac{3}{2}\pi\right\}$, $\dim(|v_x\rangle) = \dim(|v_y\rangle)$, *and*

$$\begin{cases} |v_x'\rangle\,|v_y'\rangle = |v_y\rangle\,|\overline{v_x}\rangle & \alpha = \frac{\pi}{2} \\ |v_x'\rangle\,|v_y'\rangle = |\overline{v_x}\rangle\,|\overline{v_y}\rangle & \alpha = \pi \\ |v_x'\rangle\,|v_y'\rangle = |\overline{v_y}\rangle\,|v_x\rangle & \alpha = \frac{3\pi}{2} \end{cases} \tag{36}$$

For example, the result after applying $R^{\alpha}_{|v_x\rangle\otimes|v_y\rangle}$ to the NASS state $|\psi\rangle_k$ in Eq. (15) is

$$\begin{aligned} & R^{\alpha}_{|v_x\rangle\otimes|v_y\rangle}(|\psi\rangle_k) \\ & = \sum_{i=0}^{2^n-1} \theta_i\,|i_1\cdots i_{m_1}\rangle\cdots\left|(i_{l_x+1}\cdots i_{l_x+m_x})'\right\rangle \\ & \cdots\left|(i_{l_y+1}\cdots i_{l_y+m_y})'\right\rangle\cdots|i_{l_k+1}\cdots i_{l_k+m_k}\rangle \end{aligned} \tag{37}$$

where $m_j = \dim(|v_j\rangle)$, $j = 1, 2, \ldots, k$, $m_x = m_y$, $l_l = m_1 + m_2 + \cdots + m_{l-1}$, $l = 2, \ldots, k$, and

$$\begin{cases} \left|(i_{l_x+1}\cdots i_{l_x+m_x})'\right\rangle\left|(i_{l_y+1}\cdots i_{l_y+m_y})'\right\rangle \\ = \left|i_{l_y+1}\cdots i_{l_y+m_y}\right\rangle\left|\bar{i}_{l_x+1}\cdots\bar{i}_{l_x+m_x}\right\rangle & \alpha = \frac{\pi}{2} \\ \left|(i_{l_x+1}\cdots i_{l_x+m_x})'\right\rangle\left|(i_{l_y+1}\cdots i_{l_y+m_y})'\right\rangle \\ = \left|\bar{i}_{l_x+1}\cdots\bar{i}_{l_x+m_x}\right\rangle\left|\bar{i}_{l_y+1}\cdots\bar{i}_{l_y+m_y}\right\rangle & \alpha = \pi \\ \left|(i_{l_x+1}\cdots i_{l_x+m_x})'\right\rangle\left|(i_{l_y+1}\cdots i_{l_y+m_y})'\right\rangle \\ = \left|\bar{i}_{l_y+1}\cdots\bar{i}_{l_y+m_y}\right\rangle\left|i_{l_x+1}\cdots i_{l_x+m_x}\right\rangle & \alpha = \frac{3\pi}{2} \end{cases} \tag{38}$$

A swap gate is illustrated in Figure 16. The implementation circuits for $R^{\alpha}_{|v_i\rangle\otimes|v_j\rangle}$ are shown in Figure 17.

It follows from Figure 17 that $R^{\alpha}_{|v_x\rangle\otimes|v_y\rangle}$ can be built from m_x swap gates shown in Figure 16 and m_x X gates shown in Figure 1 for $\alpha = \frac{\pi}{2}$ or $\alpha = \frac{3\pi}{2}$. When $\alpha = \pi$, $R^{\alpha}_{|v_x\rangle\otimes|v_y\rangle}$ can be built by $2m_x$ X gates. Because $m_x = \dim(|v_x\rangle) < n$, the complexity of the orthogonal rotation $R^{\alpha}_{|v_x\rangle\otimes|v_y\rangle}$ is $O(n)$.

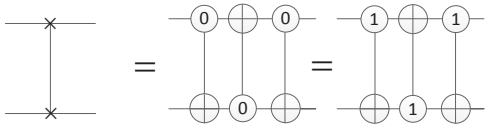

Figure 16: Swap gate. The swap gate (left) can be built using three N_{C0} gates (middle) or three N_{C1}gates(right), where N_{C0} and N_{C1} are shown in Figure 2.

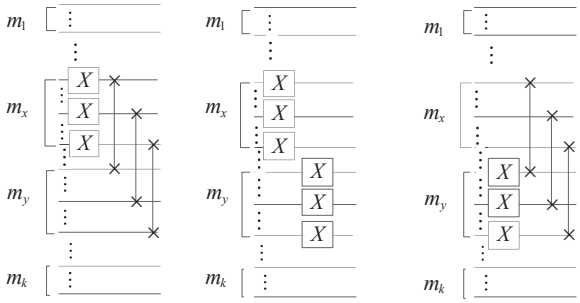

Figure 17: Implementation circuits for orthogonal rotation operators $R^{\alpha}_{|v_x\rangle\otimes|v_y\rangle}$. (a) $\alpha = \frac{\pi}{2}$. (b) $\alpha = \frac{\pi}{2}$. (c) $\alpha = \pi$ and $\alpha = \frac{3\pi}{2}$.

3.4. Translations

Definition 6. *A translation $T_{|v_x\rangle}$ for the NASS state $|\psi\rangle_k$ along the $|v_x\rangle$ axis is defined as the operator*

$$T_{|v_x\rangle}(|\psi\rangle_k) = \sum_{i=0}^{2^n-1} \theta_i \, |v_1\rangle \cdots |v_{x-1}\rangle \, |v_x{}'\rangle \, |v_{x+1}\rangle \cdots |v_k\rangle \tag{39}$$

where $|\psi\rangle_k$ represents a k-dimensional color image (see Eq. (13)), $\dim(|v_x\rangle) = m_x$. *Suppose that $|v_x\rangle = |x_1 x_2 \cdots x_{m_x}\rangle = |j\rangle$, where $j = x_1 x_2 \cdots x_{m_x}$ is the binary expansion of the integer j, then*

$$\begin{cases} |v_x{}'\rangle = |j+1\rangle & 0 \le j = x_1 x_2 \cdots x_{m_x} \le 2^{m_x} - 2 \\ |v_x{}'\rangle = |0\rangle & j = 2^{m_x} - 1 \end{cases} \tag{40}$$

For example, when $\dim(|v_i\rangle) = m_i$, $i = 1, 2, \ldots, k$, the translation opera-

tor $T_{|v_x\rangle}$ of a k-dimensional color image is also expressed as

$$\begin{aligned} T_{|v_x\rangle} &= I^{\otimes m_1} \otimes \cdots I^{\otimes m_{x-1}} \\ &\otimes \left(\left(\sum_{j=0}^{2^{m_x}-2} |j+1\rangle \langle j| \right) + |0\rangle \langle 2^m - 1| \right) \\ &\otimes I^{\otimes m_{x+1}} \cdots \otimes I^{\otimes m_k} \end{aligned} \tag{41}$$

The inside factor is called the key of implementing the translation $T_{|v_x\rangle}$ in Eq. (41):

$$T_{key} = \left(\sum_{j=0}^{2^{m_x}-2} |j+1\rangle \langle j| \right) + |0\rangle \langle 2^m - 1| \tag{42}$$

and the operator T_{key} in Eq. (42) can be implemented by two-point swappings successively as follows.

$$\begin{aligned} &|2^{m_x} - 1\rangle \leftrightarrow |0\rangle \\ &|2^{m_x} - 2\rangle \leftrightarrow |2^{m_x} - 1\rangle \\ &|2^{m_x} - 3\rangle \leftrightarrow |2^{m_x} - 2\rangle \\ &\vdots \\ &|1\rangle \leftrightarrow |2\rangle \end{aligned} \tag{43}$$

Theorem 3. *The operator T_{key} in Eq. (42) can be implemented by $2^{\mathrm{m}}-1$ two-point swapping operators. The complexity of the operator T_{key} is $O(2^m m^2)$, and the complexity of the translation $T_{|v_x\rangle}$ is also $O(2^m m^2)$, where $\dim(|v_x\rangle) = m$.*

Proof. See Appendix C. □

The quantum circuit for the translation $T_{|v_x\rangle}$ is shown in Figure 18.

Substituting $n = 5$, $k = 5$, $x = 4$ and $m_1 = m_2 = m_3 = m_4 = m_5 = 1$ into Eq. (41), we get the translation $T_{|v_4\rangle}$ for a 5D color image along $|v_4\rangle$ axis

$$T_{|v_4\rangle} = I \otimes I \otimes I \otimes (|1\rangle \langle 0| + |0\rangle \langle 1|) \otimes I \tag{44}$$

After applying the operator $T_{|v_4\rangle}$ in Eq. (44) to the image in Figure 6, the quantum circuit and the result obtained are shown in Figure 19.

Substituting $n = 5$, $k = 3$, $x = 2$, $m_1 = 2$, $m_2 = 2$, and $m_3 = 1$ into Eq. (41), we obtain

$$T_{|v_2\rangle} = I^{\otimes 2} \otimes \left(\sum_{j=0}^{2} |j+1\rangle \langle j| + |0\rangle \langle 3| \right) \otimes I \tag{45}$$

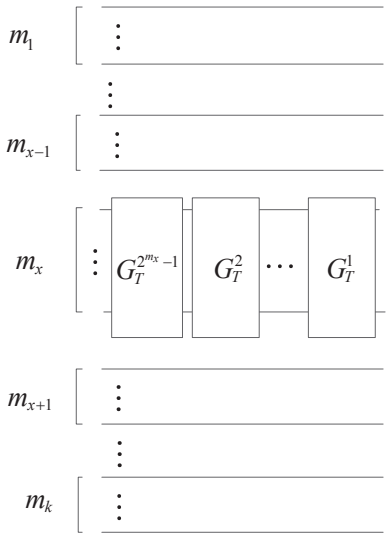

Figure 18: Implementation circuit for the translation $T_{|v_x\rangle}$, where $G_T^{2^{m_x}-1}, G_T^{2^{m_x}-2}, \cdots G_T^1$ are the circuits to implement two-point swapping successively in Eq. (43) using Gray codes.

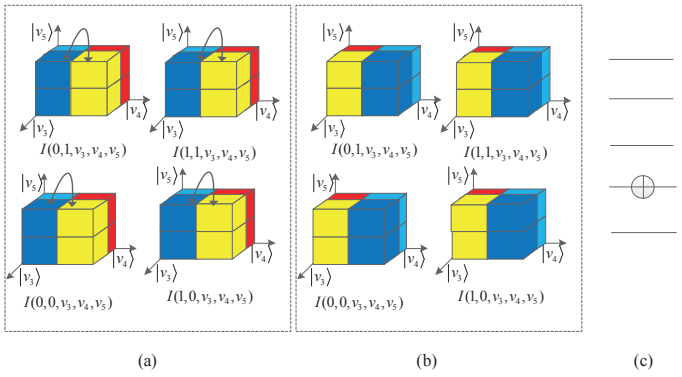

Figure 19: Translation of a 5D color image along $|v_4\rangle$ axis. (a) The original image. (b) The transformed image. (c) The implementation circuit.

which implements a translation of a 3D color image and is shown in Figure 20. The circuits in the three dashed boxes, G_T^3, G_T^2, and G_T^1, implement successively two-point swappings: $|3\rangle \leftrightarrow |0\rangle$, $|2\rangle \leftrightarrow |3\rangle$ and $|1\rangle \leftrightarrow |2\rangle$. The application of the quantum circuit in part (a) of Figure 20 to the image in Figure 5 is shown in Figure 21.

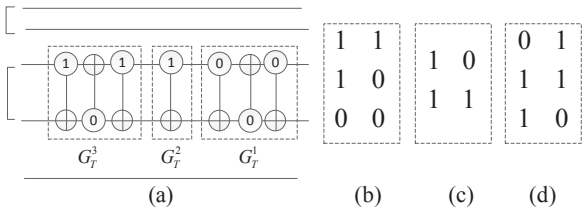

Figure 20: Implementation circuit for a 3D color image. (a) The quantum circuit. (b) Gray code for G_T^3. (c) Gray code for G_T^2. (d) Gray code for G_T^1.

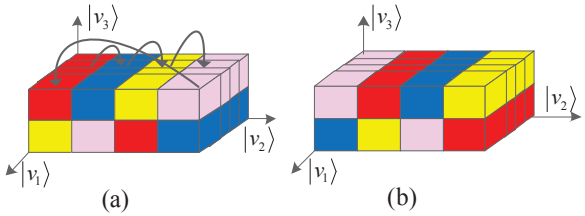

Figure 21: Translation for a 3D color image along $|v_2\rangle$ axis. (a) The original image. (b) The transformed image.

3.5. Comparison of geometric transformations

Realization of images by geometric transformations over a quantum system is a relatively new research topic. To the best of our knowledge, geometric transformations based on FRQI (GTBFRQI) [16, 17] seems to be the only available method. Compared with GTBFRQI, our method is capable of handling color and higher dimensional images, while GTBFRQI is only suitable for 2D gray images. Table 1 and Table 2 show the comparison of the two protocols, where N is the number of pixels in the image. Table 1 shows the result of our method to multidimensional color and gray images. To store an image with N pixels, our proposed method requires $\log N$ qubits, whereas GTBFRQI needs $\log N + 1$ qubits. Table 2 also highlights that our method includes new transformation functions such as local flips and translations, which were absent in GTBFRQI.

On classical computers, global operators of geometric transformations for an $\sqrt{N} \times \sqrt{N}$ image are done by $\sqrt{N} \times \sqrt{N}$-matrices, so the complexity of implementation is at least $O(N)$ [2, 6]. In our proposed quantum system, the global operators (symmetric flips, local flips, and orthogonal rotations) in Table 2 can be implemented by $O(\log N)$ gates using quantum parallel computing.

Table 1: Image types for geometric transformations.

	GTBNASS	GTBFRQI
Image types	Multidimensional color and gray image	2D gray image
Qubit number of image storage	$\log N$	$\log N + 1$

Table 2: Complexity of geometric transformations.

	GTBNASS	GTBFRQI
Two-point swapping	$O(2\log N)$	$O(2\log N + 2)$
Symmetric flip	$O(\log N)$	$O(\log N + 1)$
Local flip	$O(\log N)$	–
Orthogonal rotation	$O(\log N)$	$O(\log N + 1)$
Translation	$< O(N \log N)$	–

4. Experiments of geometric transformations

In the absence of the quantum computer to implement proposed geometric transformations, experiments of quantum images are simulated on a classical computer. The quantum images are stored in column vectors and geometric transformations are implemented using unitary matrices in Matlab.

A 128×128 image is regarded as the input image shown in Figure 22. Results of symmetric flips are showed in (a) and (b) of Figure 23. The operators of (a) and (b) of Figure 23 are $G_F^{|X\rangle}{=}X^{\otimes 7}{\otimes}I^{\otimes 7}$ and $G_F^{|Y\rangle}{=}I^{\otimes 7}{\otimes}X^{\otimes 7}$.

Figure 22: Original image

$G_{LF}^{|v_1\rangle v(2,1,1)}$ and $G_{LF}^{|v_1\rangle v(2,1,0)}$ are the operators to flip the lower part and the upper part of the original image shown in Figure 22, respectively. Applications of $G_{LF}^{|v_1\rangle v(2,1,1)}$ and $G_{LF}^{|v_1\rangle v(2,1,0)}$ to the original image of Figure 22 are showed in (a) and (b) of Figure 24.

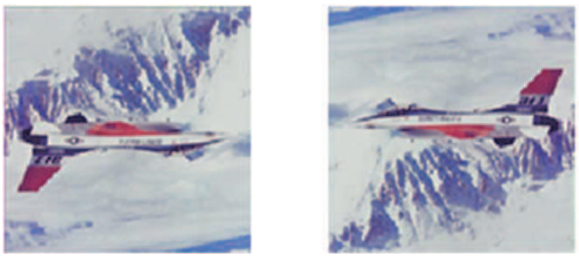

(a) (b)

Figure 23: Experiments of symmetric flips. (a) Flip along X axis. (b) Flip along Y axis.

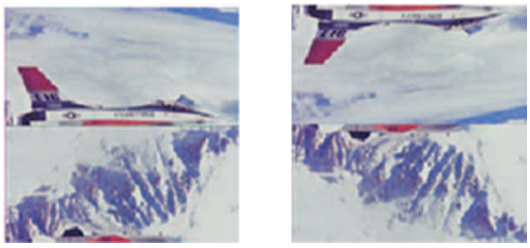

(a) (b)

Figure 24: Experiments of local flips. (a) Local flip for the lower part. (b) Local flip for the upper part.

Application of the orthogonal rotations $R^{\pi/2}_{|v_x\rangle\otimes|v_y\rangle}$, $R^{\pi}_{|v_x\rangle\otimes|v_y\rangle}$ and $R^{3\pi/2}_{|v_x\rangle\otimes|v_y\rangle}$ on the image of Figure 22 are showed in Figure 25.

(a) (b) (c)

Figure 25: Experiments of orthogonal rotations. (a) Rotation by $\frac{\pi}{2}$. (b) Rotation by π. (c) Rotation by $\frac{3\pi}{2}$.

The translation operator $T_{|v_y\rangle} = \left(\left(\sum_{j=0}^{2^7-2} |j+1\rangle\langle j|\right) + |0\rangle\langle 2^7-1|\right) \otimes I^{\otimes 7}$ is applied repeatedly 10 times and 30 times on the image of Figure 22. Experimental data are showed in Figure 26.

(a) (b)

Figure 26: Experiments of translations. (a) Translation of 10 pixels along Y axis. (b) Translation of 30 pixels along Y axis.

5. Conclusions

In this study, we have shown how an n-qubit NASS state represents a k-dimensional color image of $N = 2^n$ pixels, which demonstrates the vast capacity of NASS to store information. For a multidimensional color image based on NASS, the quantum circuits described in this study provide a convenient and efficient method for implementing geometric transformations of two-point swappings, symmetric flips, local flips, orthogonal rotations, and translations. The complexity analysis of the geometric transformations has shown that the global operators (symmetric flips, local flips, orthogonal rotations) can be implemented by $O(n)$ gates, and the local operators (two point swappings) by $O(n^2)$ gates. This proves that the global operators are faster than the local ones, while it is the opposite in classical image processing. The translation of a k-dimensional color image is achieved without additional storage space due to quantum parallel computing, which is difficult to achieve on a classical computer. The complexity of all geometric transformations (both global and local) are lower than $O(N \log N)$, where $N = 2^n$ is the number of pixels, which implies that a geometric transformation can be constructed with a polynomial number of single-qubit and two-qubit gates. The results of simulated experiments further confirm the validity of proposed

geometric transformations. The proposed quantum scheme is one step towards more applications on quantum images with relative low complexity. It is hoped that similar common transformations such as affine and non-rigid transformations can be implemented.

Appendix A. Proof of Theorem 1

Proof. Note that g_i and g_{i+1} $(1 \leq i \leq m-1)$ differ by exactly one bit, say at the jth bit, i.e.,

$$\begin{cases} g_i = i_1 \cdots i_j \cdots i_n \\ g_{i+1} = i_1 \cdots \bar{i}_j \cdots i_n \end{cases} \tag{A.1}$$

where $\bar{i}_j = 1 - i_j$, $1 \leq j \leq n$.

Note that the quantum circuit X sends $|i_j\rangle$ to $|\bar{i_j}\rangle$, therefore the $C^n(X_j)$ gate in Figure 3 implements that

$$C^n(X_j)\,|g_i\rangle = |g_{i+1}\rangle \tag{A.2}$$

$$C^n(X_j)\,|g_{i+1}\rangle = |g_i\rangle \tag{A.3}$$

and for $|x\rangle \neq |g_i\rangle, |g_{i+1}\rangle$,

$$C^n(X_j)\,|x\rangle = |x\rangle \tag{A.4}$$

Denote this $C^n(X_j)$ by C_i, i.e. $C_i|g_i\rangle = |g_{i+1}\rangle$, $C_i|g_{i+1}\rangle = |g_i\rangle$, and C_i fixes other $|g_j\rangle's$.

Let $C_T = C_1 C_2 \cdots C_{m-2} C_{m-1} C_{m-2} \cdots C_1$. From (A.2), (A.3), and (A.4) it follows that C_T is built by $2m-3$ gates $C^n(X_y)$ $(1 \leq y \leq n)$, which implements the transformations $|g_1\rangle \to |g_2\rangle \to \cdots \to |g_m\rangle$ and $|g_{m-1}\rangle \to |g_{m-2}\rangle \to \cdots \to |g_1\rangle$, and we have

$$\begin{cases} C_T\,|s\rangle = C_T\,|g_1\rangle = |g_m\rangle = |t\rangle \\ C_T\,|t\rangle = C_T\,|g_m\rangle = |g_1\rangle = |s\rangle \\ C_T\,|x\rangle = |x\rangle \end{cases} \tag{A.5}$$

where $|x\rangle \neq |s\rangle$ and $|x\rangle \neq |t\rangle$. Thus, by applying C_T to the NASS state $|\psi\rangle_k$ in Eq. (13), we have

$$\begin{aligned} C_T(|\psi\rangle_k) &= \sum_{i=0}^{2^n-1} \theta_i C_T\,|i\rangle \\ &= \theta_s\,|t\rangle + \theta_t\,|s\rangle + \sum_{i=0, i\neq s,t}^{2^n-1} \theta_i\,|i\rangle \end{aligned} \tag{A.6}$$

By comparing (A.6) with Eq. (21), we have proved that $C_T = G_T$, i.e., a sequence of quantum gates $C^n(X_y)$, $1 \leq y \leq n$, implements the two-point swapping G_T.

Since s and t differ in at most n locations, there exists a Gray code such that $m \leq n+1$. In addition, the $C^n(X_y)$ gate is implemented using $O(n)$ single-qubit and controlled-NOT (i.e., N_{C1} in Figure 2)) gates [22, 16]. C_T is built by $2m-3$ gates $C^n(X_y)$ $(1 \leq y \leq n)$, thus the complexity of C_T is $O(n^2)$, i.e., the complexity of a two-point swapping operator G_T is also $O(n^2)$. □

Appendix B. Proof of Theorem 2

Proof. From definition 3, we see that a symmetric flip of a k-dimensional image with 2^n pixels requires a swapping of 2^n pixel points, thus the operator $G_F^{v_i}$ can be implemented using 2^{n-1} two-point swappings, i.e.,

$$T = \prod_{i=1}^{2^{n-1}} G_{T_i} \tag{B.1}$$

and

$$G_F^{|v_j\rangle}|\psi\rangle_k = T|\psi\rangle_k \tag{B.2}$$

where G_{T_i} is the ith two-point swapping operator and $|\psi\rangle_k$ is the NASS state in Eq. (13). Since both operators are unitary, it is easy to see that

$$G_F^{|v_j\rangle} = T = \prod_{i=1}^{2^{n-1}} G_{T_i} \tag{B.3}$$

which implies that the operator T can be implemented by 2^{n-1} two-point swappings (see Figure 10). Therefore, the complexity of the symmetric flip is also $O(n)$. □

Appendix C. Proof of Theorem 3

Proof. Set

$$|\psi\rangle = \sum_{j=0}^{2^m-1} \alpha_j |j\rangle \tag{C.1}$$

Application of T_{key} to $|\psi\rangle$ gives that

$$T_{key}\,|\psi\rangle = \alpha_{2^m-1}\,|0\rangle + \sum_{j=0}^{2^m-2} \alpha_j\,|j+1\rangle \tag{C.2}$$

Define a sequence of two-point swappings as follows.

$$\begin{array}{l} G_T^{2^m-1} : |2^m-1\rangle \leftrightarrow |0\rangle \\ G_T^{2^m-2} : |2^m-2\rangle \leftrightarrow |2^m-1\rangle \\ G_T^{2^m-3} : |2^m-3\rangle \leftrightarrow |2^m-2\rangle \\ \vdots \\ G_T^{1} : |1\rangle \leftrightarrow |2\rangle \end{array} \tag{C.3}$$

Applying $(G_T^1 \cdots G_T^{2^m-2} G_T^{2^m-1})$ to $|\psi\rangle$ in (C.1), we obtain

$$(G_T^1 \cdots G_T^{2^m-2} G_T^{2^m-1})\,|\psi\rangle = \alpha_{2^m-1}\,|0\rangle + \sum_{j=0}^{2^m-2} \alpha_j\,|j+1\rangle \tag{C.4}$$

It follows from (C.2) and (C.4) that $G_T^1 \cdots G_T^{2^m-2} G_T^{2^m-1} = T_{key}$, i.e., the operator T_{key} in Eq. (42) can be implemented by $2^{\mathrm{m}}-1$ two-point swappings.

By Theorem 1 we know that the complexity of $G_T^1 \cdots G_T^{2^m-2} G_T^{2^m-1}$ is $O(2^m m^2)$, i.e., the complexity of T_{key} is $O(2^m m^2)$. From Figure 18 we see that the complexity of $T_{|v_x\rangle}$ is the same as that of T_{key}, i.e., the complexity of $T_{|v_x\rangle}$ is also $O(2^m m^2)$. □

Acknowledgments

This work is supported by National Natural Science Foundation of China (Nrs. 61463016, 61462026, 11271138, 11531004), Simons Foundation Grant No. 198129, Program for New Century Excellent Talents in University under Grant No. NCET-13-0795, Landing project of science and technique of colleges and universities of Jiangxi Province under Grant No. KJLD14037, Training program of academic and technical leaders of Jiangxi Province under Grant No. 20153BCB22002, Natural Science Foundation of Jiangxi Province (No. 20151BAB207019), the advantages of scientific and technological innovation team of Nanchang City under Grant No. 2015CXTD003, the research funds of East China Jiaotong University (15XX02 and 15QT02), and an award of China Scholarship Council.

References

[1] J. Ahn, T.C. Weinacht, and P.H. Bucksbaum, Information storage and retrieval through quantum phase, Science, 287(2000) 463-465.

[2] E.R. Arce-Santana, A. Alba, Image registration using Markov random coefficient and geometric transformation fields, Pattern Recognition, 42(8) (2009) 1660-1671.

[3] A. Barenco, C.H. Bennett, et al., Elementary gates for quantum computation, Phys. Rev. A, 52 (1995) 3457-3467.

[4] D. Deutsch, Quantum theory, the Church-Turing principle and the universal quantum computer, Proc. Roy. Soc. London A, 400 (1985), pp. 97-117.

[5] D.P. DiVincenzo, Two-bit gates are universal for quantum computation, Phys. Rev. A, 51 (1995) 1015-1022.

[6] S.R. Dooley, R.W. Stewart, T.S. Durrani, et al., Setarehdan et al. Efficient Implementation of Accurate Geometric Transformations for 2-D and 3-D Image Processing, IEEE Trans. Image Processing, 13(8) (2004) 1060-1065.

[7] R.P. Feynman, Simulating physics with computers, Int. J. Theo. Phys., 21 (1982) 467-488.

[8] R.P. Feynman. Quantum mechanical computers, Foundations of physics, 1986, 16(6) (1986) 507-531

[9] L.K. Grover, A fast quantum mechanical algorithm for database search, Proceedings of the 28th Annual ACM Symposium on Theory of Computing, 1996, pp. 212-219.

[10] L. Gyongyosi, S. Imre, Geometrical analysis of physically allowed quantum cloning transformations for quantum cryptography, Inform. Sci., 285(20) (2014) 1-23.

[11] A.M. Iliyasu ,P.Q. Le, F. Dong, et al., Watermarking and authentication of quantum images based on restricted geometric transformations, Inform. Sci., 186 (2012) 126-149.

[12] A.M. Iliyasu, Towards Realising Secure and Efficient Image and Video Processing Applications on Quantum Computers, Entropy, 15(8) (2013) 2874-2974.

[13] A.M. Iliyasu, P.Q. Le, F. Dong, et al. A framework for representing and producing movies on quantum computers, Int. J. Quant. Inf., 9(6) (2011) 1459-1497.

[14] S. Lloyd, A potentially realizable quantum computer, Science, 261(5128) (1993) 1569-1571

[15] P.Q. Le, F. Dong, K. Hirota, A flexible representation of quantum images for polynomial preparation, image compression, and processing operations, Quantum Inf. Process, 10 (2011) 63-84.

[16] P.Q. Le, A.M. Iliyasu, F. Dong, et al., Fast geometric transformations on quantum images, IAENG Inter. J. Appl. Math., 40(3), (2010) 113-123.

[17] P.Q. Le, A.M. Iliyasu, F. Dong, et al., Strategies for designing geometric transformations on quantum images, Theo. Computer Sci., 412 (15) (2011) 1406-1418.

[18] H.S. Li, Q. Zhu, L. Song, et al., Image storage, retrieval, compression and segmentation in a quantum system, Quantum Inf. Process., 12 (2013) 2269-2290.

[19] H.S. Li, Q. Zhu, R.G. Zhou, et al., Multi-dimensional color image storage and retrieval for a normal arbitrary quantum superposition state, Quantum Inf. Process., 13(4) (2014), 991-1011.

[20] H.S. Li, Q. Zhu, R.G. Zhou, et al., Multidimensional color image storage, retrieval, and compression based on quantum amplitudes and phases, Inform. Sci., 273 (2014), 212-232.

[21] G.L. Long, Y. Sun, Efficient Scheme for Initializing a quantum register with an arbitrary superposed state, Phys. Rev. A, 64 (2001) 014303.

[22] M.A. Nielsen, I.L. Chuang, Quantum Computation and Quantum Information, Cambridge University Press, Cambridge, 2000.

[23] C.Y. Pang, R.G. Zhou, C.B. Ding et al., Quantum search algorithm for set operation, Quantum Inf. Process., 12 (2013) 481-492.

[24] P.W. Shor, Algorithms for quantum computation: Discrete logarithms and factoring, Proceedings of the 35th Annual IEEE Symposium on Foundations of Computer Science, 1994, pp. 124-134.

[25] M. Song, D. Tao, C. Chen, et al., Color to Gray: Visual Cue Preservation, IEEE Transactions on Pattern Analysis and Machine Intelligence (T-PAMI), 32(9) (2010) 1537-1552.

[26] M. Song, D. Tao, J. Bu, C. Chen, Y. Yang, Color-to-Gray based on Chance of Happening Preservation, Neurocomputing, 119 (2013) 222-231.

[27] S.E. Venegas-Andraca, S. Bose, Storing, processing and retrieving an image using quantum mechanics, Proc. SPIE Conf. Quantum Inf. Comput., 2003, pp. 137-147.

[28] S.E. Venegas-Andraca, J.L. Ball, Processing images in entangled quantum systems, Quantum Inf. Process, 9(1) (2010) 1-11.

[29] F. Xue, S. Xu, C. He, et al., Towards efficient support relation extraction from RGBD images, Inform. Sci., 320(1) (2015) 320-332.

[30] Y.G. Yang, X. Jia, S.J. Sun, et al., Quantum cryptographic algorithm for color images using quantum Fourier transform and double random-phase encoding, Inform. Sci., 277(1) (2014) 445-457.

[31] A.C. Yao, Quantum circuit complexity, In Proceedings of the 34th Annual Symposium on Foundations of Computer Science, Los, Angeles, 1993 352-361.

[32] A. Younes, Enhancing the security of quantum communication by hiding the message in a superposition, Inform. Sci. 181 (2011) 329-334.

[33] R.G. Zhou, Q. Wu, M.Q. Zhang, et al., Quantum Image Encryption and Decryption Algorithms Based on Quantum Image Geometric Transformations, Int. J. Theo. Phys., 52(6) (2013) 1802-1817.